Electronic Supplementary Material (ESI) for Journal of Materials Chemistry A.

Supporting Information

Alkali-promoted indium oxide as highly active and selective catalyst for the photo-thermal CO$_2$ hydrogenation

Xinhuilan Wang [a], Alejandra Rendón-Patiño [a], Jean Marcel R. Gallo [a], Diego Mateo* [a], and Jorge Gascon* [a]

[a] Advanced Catalytic Materials (ACM), KAUST Catalysis Center (KCC), King Abdullah University of Science and Technology (KAUST), Thuwal 23955-6900, Saudi Arabia.

E-mail: diego.mateo@kaust.edu.sa; jorge.gascon@kaust.edu.sa

1. Catalyst Characterization

Powder X-ray diffraction (PXRD) analysis was conducted employing a Bruker D8 diffractometer configured in the Bragg-Brentano geometry. Cu Kα radiation (λ=1.5418 Å) was utilized, with operational parameters set at 40 kV and 40 mA for voltage and current respectively. Data collection spanned the 2θ range from 10 to 80 °, with increments of 0.02 ° and a time of 7 seconds per step.

Thermogravimetric (TG) measurements were recorded in an air atmosphere employing a Mettler-Toledo thermal analyzer. The temperature was ramped at a rate of 5 °C per minute within the range of 25 °C to 800 °C, while maintaining a gas flow of 25 mL · min^{-1}.

N$_2$ adsorption-desorption measurements were performed using a Micromeritics ASAP 2040 instrument at 77 K. Prior to the analysis, the catalysts underwent a degassing process under vacuum at 150 °C for 720 minutes.

The UV-Vis spectra were conducted by using a JASCO V-670 spectrophotometer. The diffuse reflectance spectra were obtained in a range of 300 – 1500 nm using halogen and deuterium lamps as light sources.

Raman spectroscopy was performed using a confocal Raman microscope WITec Apyron equipped with a 532 nm laser and power of 10 mW. The measurements were carried out using an objective lens with a magnification of 50x, and a grating of 1800 g/mm.

The CO_2 temperature-programmed desorption (CO_2-TPD) analyses were analyzed using a Micromeritics AutoChem 2920 unit. Initially, 200 mg of catalyst was preheated with helium at 200 °C for 60 minutes, followed by cooling to 50 °C. Subsequently, the catalyst was exposed to a CO_2 flow for 60 minutes. To eliminate physically adsorbed CO_2, the treated catalyst underwent helium flushing at the same temperature for 30 minutes. Following this, the catalyst was subjected to heating in a helium flow up to 800 °C, with a heating rate of 10 °C $\cdot$ min^{-1}, to observe the CO_2-TPD signal.

In situ diffuse reflectance infrared Fourier transform spectroscopy (DRIFTS) measurements were registered using the Kubelka-Munk mode on a Thermo Scientific Nicolet 6700 series Fourier transform infrared (FT-IR) spectrometer equipped with a Harrick Praying Mantis High-Temperature reaction chamber. The sample was placed into the catalyst bed and packed. Before the collection of spectra, the sample was preheated to 200 °C under a He flow of 20 mL $\cdot$ min^{-1}, and the background spectra were collected with 248 scans at 4 cm^{-1} resolution. After that, a mixture of H_2 and CO_2 (4:1) was introduced into the chamber at a flow of 20 mL $\cdot$ min^{-1}. Once the reaction chamber was purged, it was pressurized to 10 bar. IR spectra were recorded with 64 scans at 4 cm^{-1} resolution every 2 min in the temperature range from 20 °C to 350 °C (ramp rate 3 °C$\cdot$min^{-1}). To investigate the effect of illumination on both the reaction pathway and intermediates, light was introduced into the reaction chamber during the DRIFTS measurements using a white LED source (UHP-T-WCS-DI, Prizmatrix).

The CO_2 temperature-programmed desorption (CO_2-TPD) analyses were performed using the same equipment as the above-mentioned *in-situ* DRIFTS experiments. Prior to collecting the background, the sample was preheated with a flow of helium at 200 °C for 30 minutes. The background spectra were collected with 248 scans at 4 cm^{-1} resolution when sample cooled down to 50 °C. After that, the sample was exposed to a flow of CO_2 for 60 minutes and then flushed with helium for 30 minutes at 50 °C. Subsequently, the temperature was increased from 50 to 600 °C at a ramping rate of 5 °C$\cdot$min^{-1} under a flow of helium. During this stage, IR spectra were recorded with 64 scans at 4 cm^{-1} resolution every 2 min. Meanwhile, the corresponding gas phase evolution was monitored via INFICON Transpector CPM100 mass spectrometry (MS).

In the case of hydrogen temperature-programmed reduction (H_2-TPR) analyses, the samples were initially pretreated at 200 °C for 30 minutes under He flow. After cooling down to room temperature, the H_2-TPR measurement was performed by recording the amount of H_2 consumption via INFICON Transpector CPM100 mass spectrometry (MS) while heating the catalyst from 20 °C to 600 °C at a rate of 5 °C $\cdot$ min^{-1} under a gas flow of 6 vol% H_2/Ar. The H_2-TPR measurement was conducted both under dark and light conditions using a white LED source, as previously indicated.

X-ray photoelectron spectroscopy (XPS) measurements were performed using a Kratos Axis Ultra DLD instrument equipped with a monochromatic $Al_{K\alpha}$ X-ray source (hv=1486.71 eV) operating at 150 W under ultra-high vacuum ($\approx 10^{-9}$ mbar). Photoelectron peak C1s (284.8 eV for adventitious carbon) was used for binding energy correction.

Dark-field imaging was conducted using scanning transmission electron microscopy (STEM) with a high-angle annular dark-field (HAADF) detector. The STEM-HAADF data were acquired using a convergence angle of 18.2 mrad and an inner angle of 50 mrad for HAADF. The image size was set to 2048×2048 pixels, with a dwell time of 8 μs. Furthermore, a combination of X-ray energy dispersive spectrometer (XEDS) and DF-STEM imaging was employed to obtain STEM-EDS spectral image datasets. The images were configured to a size of 1024×1024 pixels, with a dwell time of 4 μs and 100 frames. Subsequently, the generated maps of In, O and Cs underwent mild filtering using a Gaussian filter (σ = 0.5) and were represented in weight percent (wt %). All STEM samples were prepared on dry copper grids coated with a lacey Carbon film (200 mesh).

2. Supplementary Figures
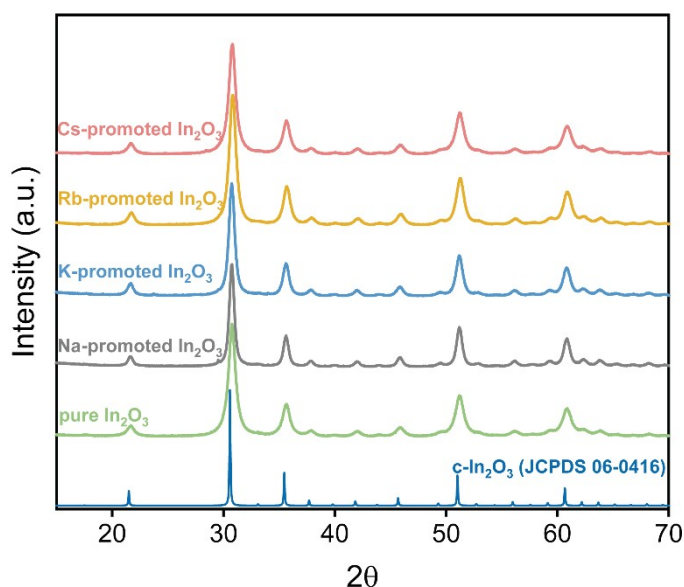
Fig S1. PXRD patterns of pure In_2O_3 and alkali-promoted In_2O_3.
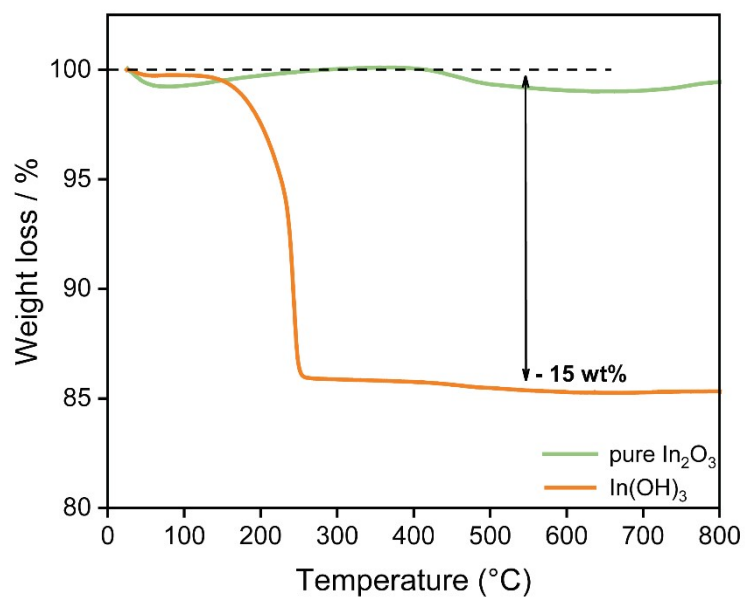
Fig S2. TGA of In(OH)$_3$ precursor and pure In$_2$O$_3$.
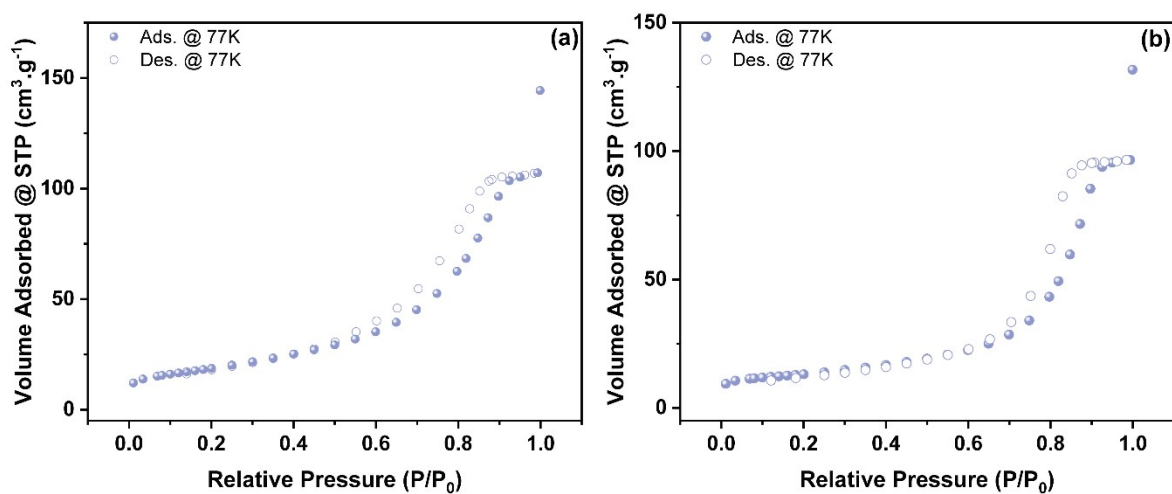
Fig S3. N$_2$ adsorption isotherms of a) pure In$_2$O$_3$ and b) Cs-promoted In$_2$O$_3$ at 77 K.

Table S1. Specific surface areas of pure and Cs-promoted In$_2$O$_3$.

Sample	Specific surface area
Pure In$_2$O$_3$	67 m^2 g^{-1}
Cs-promoted In$_2$O$_3$	44 m^2 g^{-1}
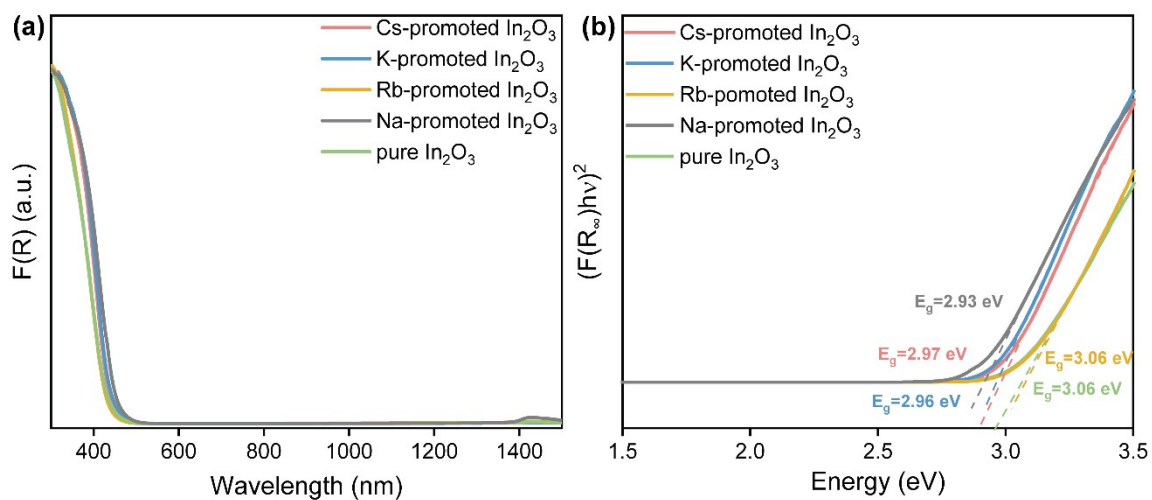
Fig S4. a) UV-vis-NIR absorption spectra and b) calculated band gap values of alkali-promoted and pure In$_2$O$_3$.
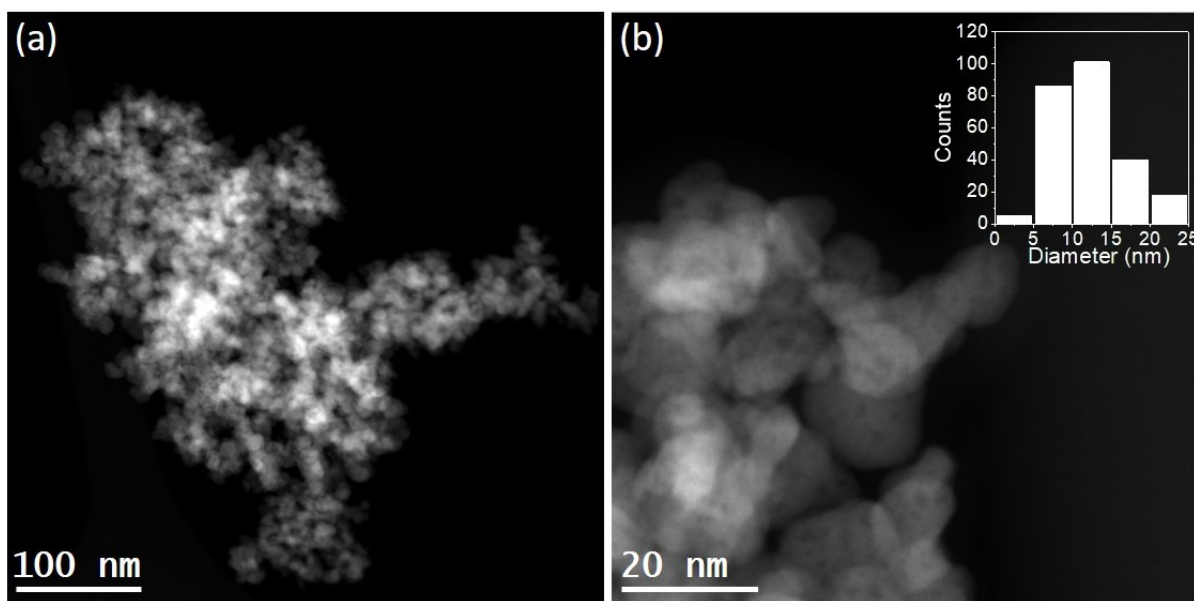
Fig S5. STEM images of pure In$_2$O$_3$ at a) low and b) high magnification. Inset in b) corresponds to the particle size distribution.
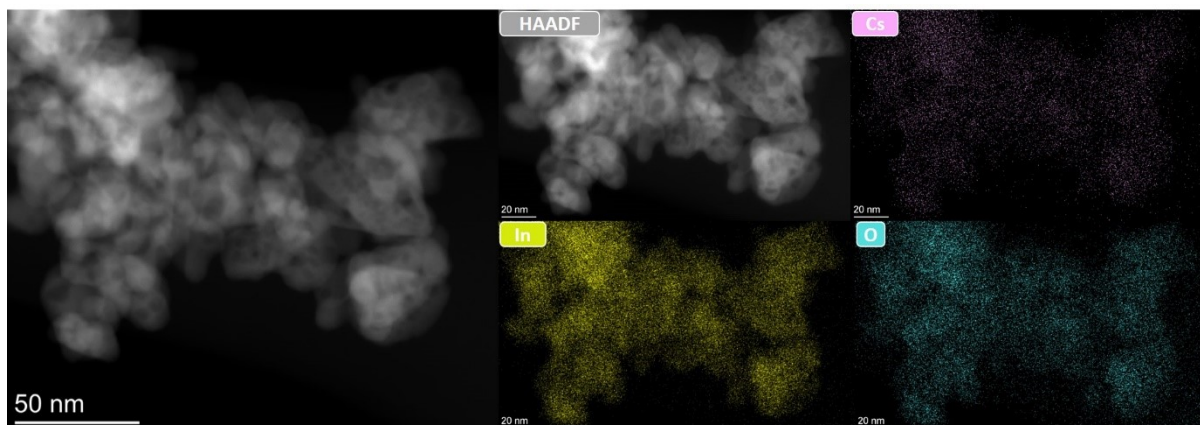
Fig S6. STEM images of Cs-promoted In$_2$O$_3$ with elemental mapping by EDX.
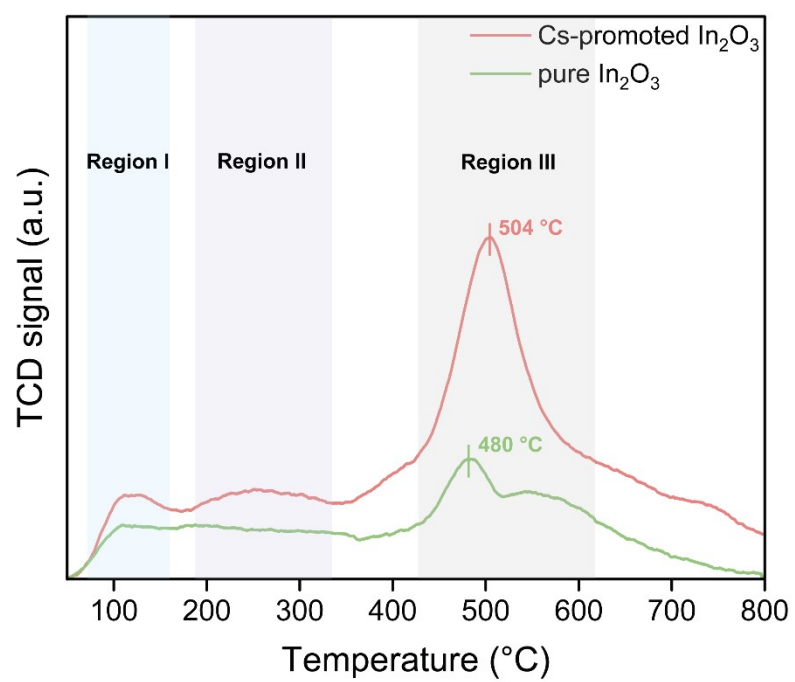
Fig S7. CO$_2$-TPD profiles of pure and Cs-promoted In$_2$O$_3$.
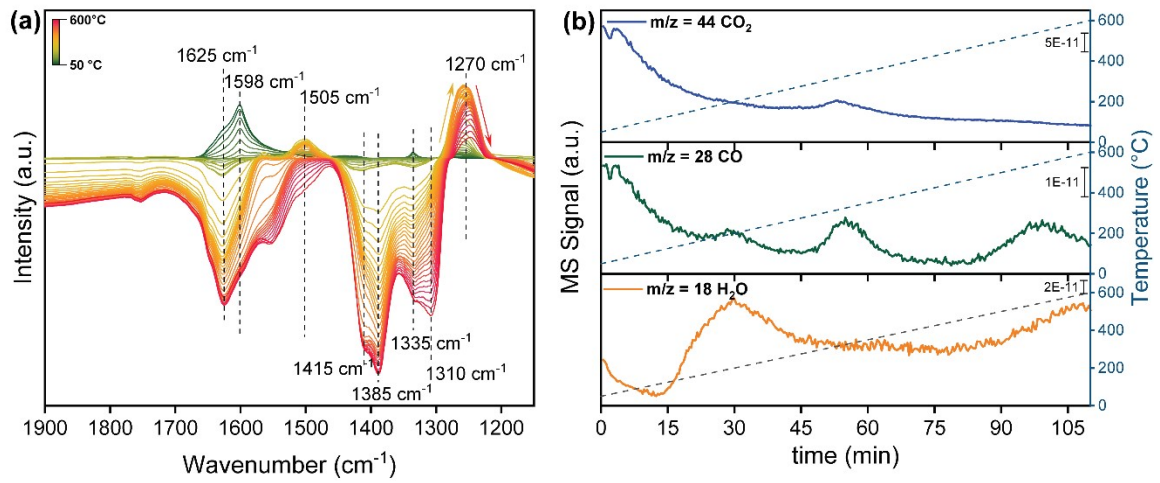
Fig S8. a) In-situ DRIFTS spectra of Cs-promoted In_2O_3 catalyst and b) corresponding MS signal.
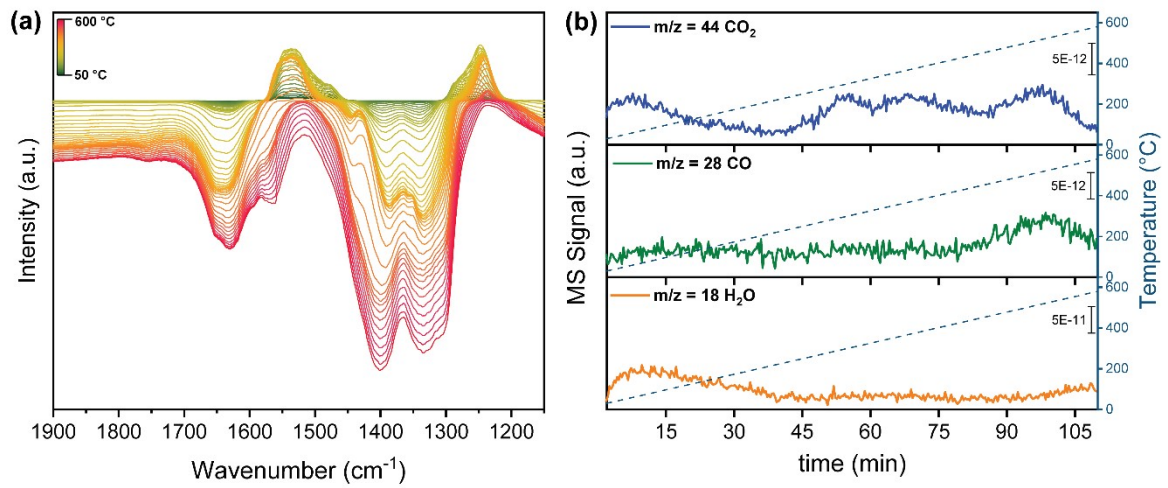
Fig S9. a) In-situ DRIFTS spectra of pure In_2O_3 catalyst and b) corresponding MS signal.
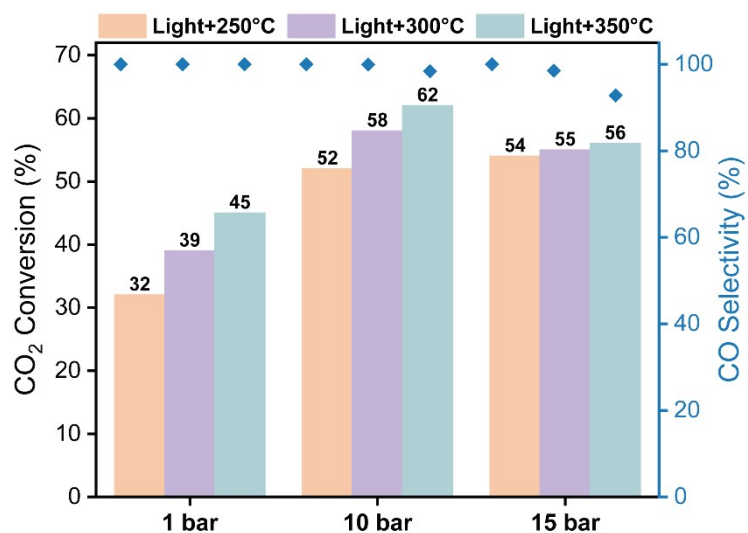
Fig S10. Study of the effect of pressure on the photo-thermal RWGS reaction over Cs-promoted In_2O_3 with external heating at 250, 300 and 350 °C. Reaction conditions: 3.3 W·cm^{-2} light intensity, GHSV = 15000 mL·h^{-1}·g^{-1}.
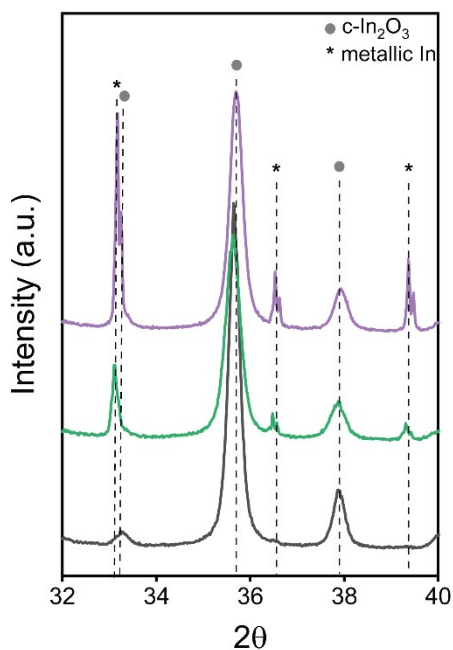
Fig S11. PXRD patterns of spent Cs-promoted In_2O_3 samples after photo-thermal RWGS reaction at 1 (black line), 10 (green line) and 15 bar (purple line) and 350 °C.
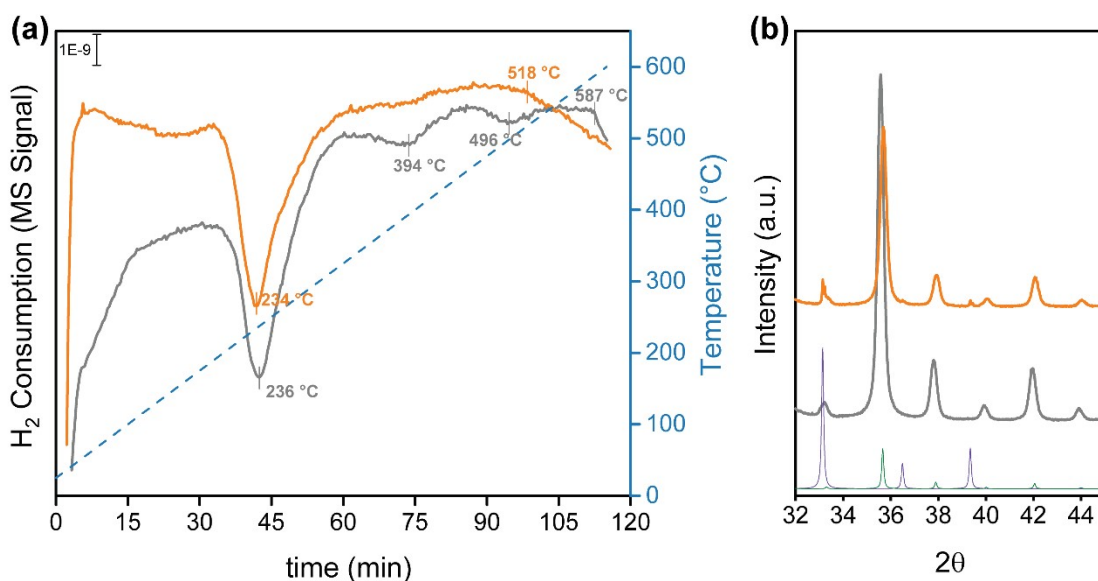
Fig S12. a) H$_2$-TPR of Cs-promoted In$_2$O$_3$ under dark (grey line) and light irradiation (orange line) conditions. b) PXRD patterns of spent Cs-promoted In$_2$O$_3$ samples after H$_2$-TPR under dark (grey line) and light irradiation (orange line) conditions. Simulated XRD patterns for c-In$_2$O$_3$ (green line) and metallic indium (purple line) are included for reference.
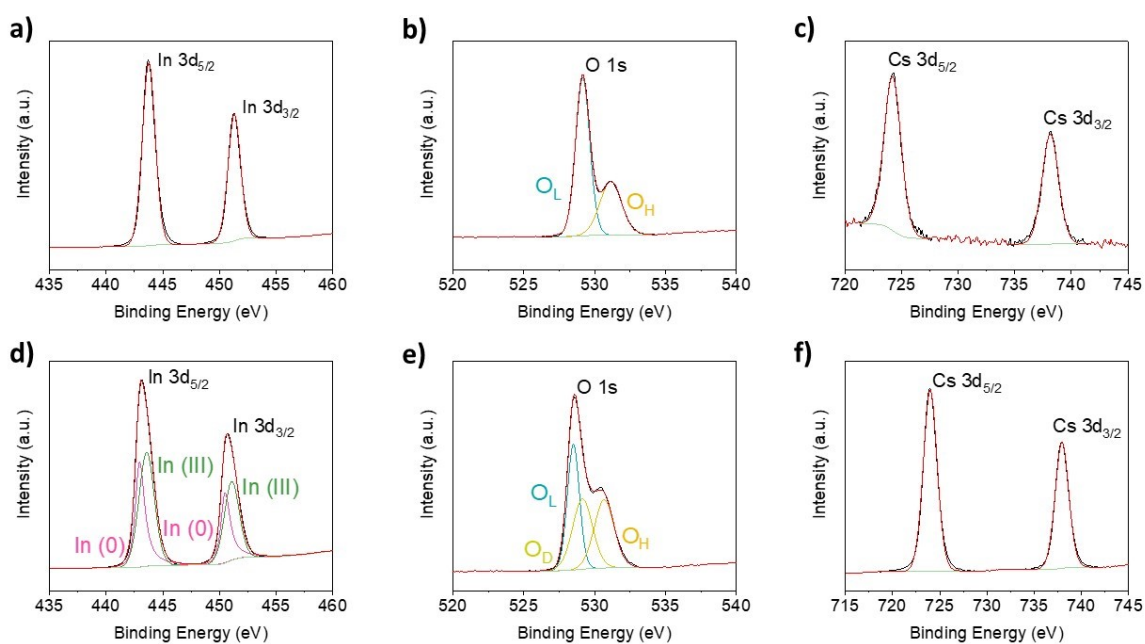
Fig S13. XPS measurements of fresh (top) and spent (bottom) Cs-promoted In$_2$O$_3$ sample.
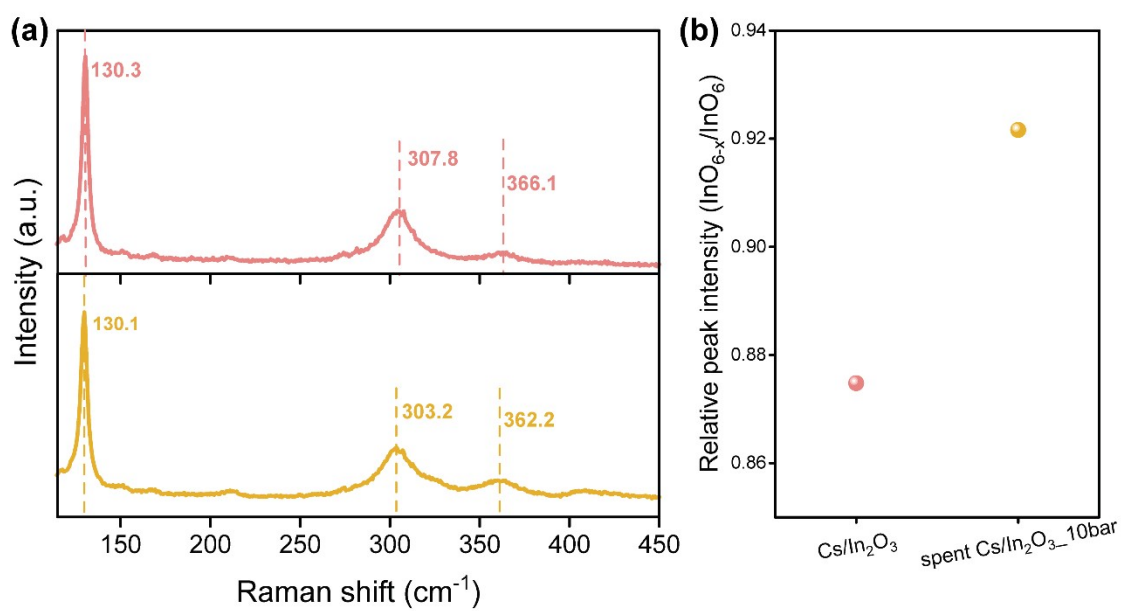
Fig S14. a) Raman spectra of fresh (red line) and spent (yellow line) Cs-promoted In_2O_3 catalysts. b) Relative peak intensity ratio between InO_{6-x} and InO_6.
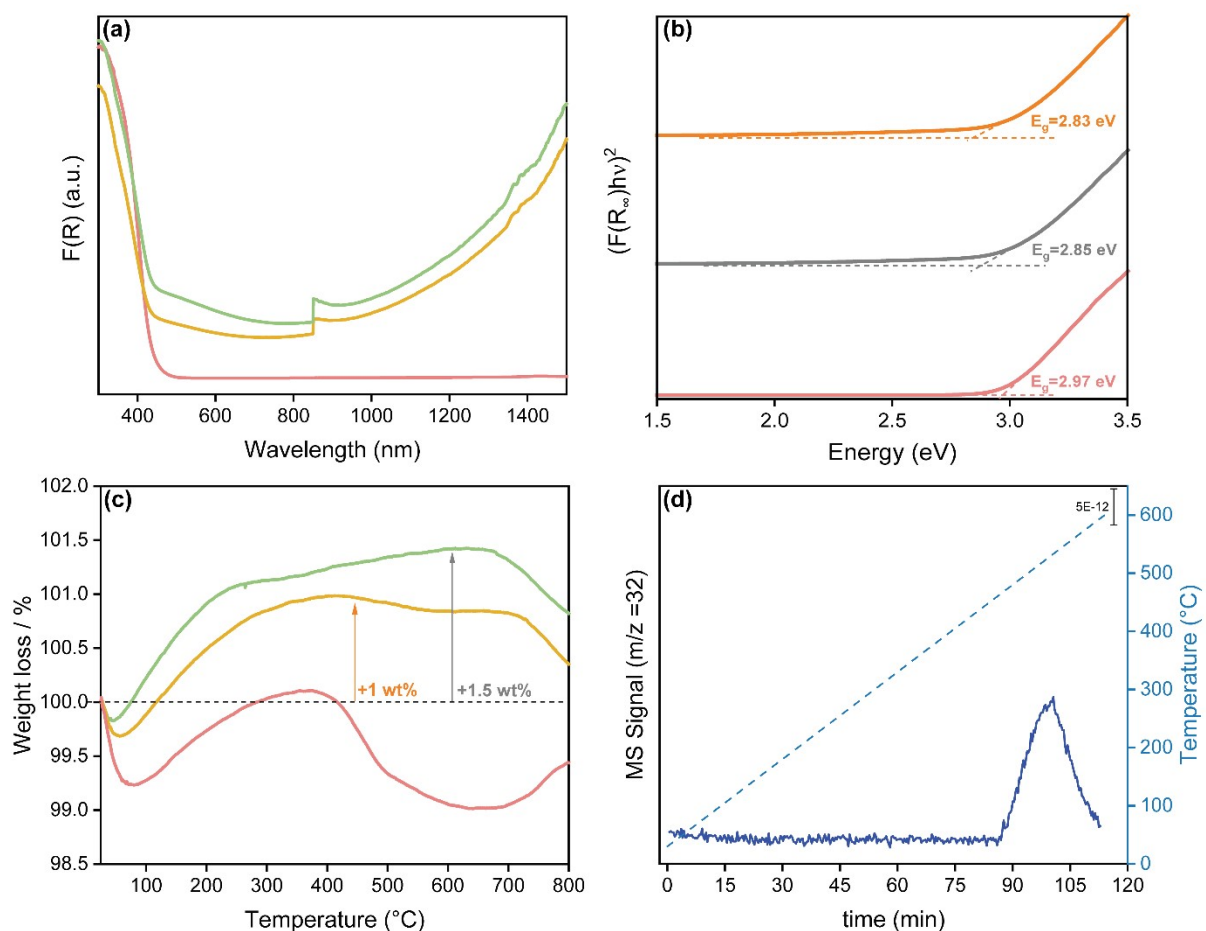
Fig S15. a) UV-vis-NIR absorption spectra of fresh Cs-promoted In_2O_3 (red line), Cs-promoted In_2O_3 after illumination w/o external heating (yellow line) and Cs-promoted In_2O_3 after illumination at 250°C (green line). b) calculated band gap values of fresh Cs-promoted In_2O_3 (red line), spent Cs-promoted In_2O_3 after photothermal reaction at 250 °C and 1 bar (grey line) and spent Cs-promoted In_2O_3 after photothermal reaction at 250 °C and 10 bar (orange line). c) TGA curves of fresh Cs-promoted In_2O_3 (red line), Cs-promoted In_2O_3 after illumination w/o external heating (yellow line) and Cs-promoted In_2O_3 after illumination at 250°C (green line). d) MS results for gas phase analysis of Cs-promoted In_2O_3 under light illumination.
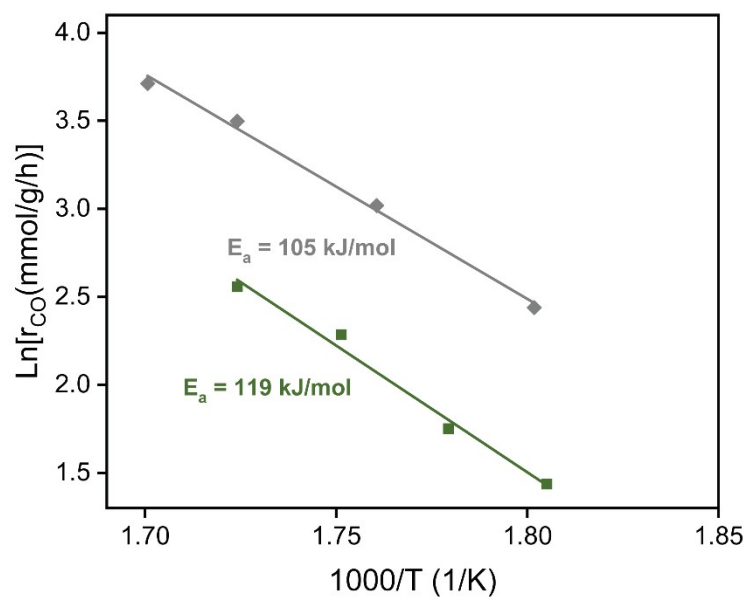
Fig S16. Calculated activation energies of Cs-promoted In_2O_3 under light (grey line) and dark (olive line).
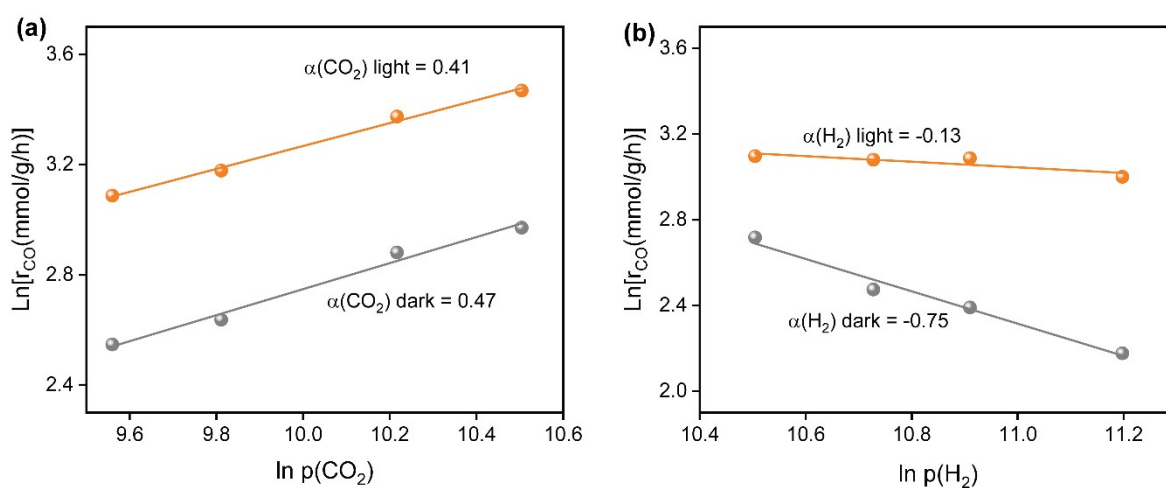
Fig S17. Dependence of CO production rate on the partial pressures of a) CO_2 and b) H_2 under light irradiation (orange spheres) and dark conditions (grey spheres), over Cs-promoted In_2O_3. Reaction conditions: 3.3 $W \cdot cm^{-2}$ light intensity, GHSV = 15000 $mL \cdot h^{-1} \cdot g^{-1}$, 1 bar.

3. Supplementary Tables

Table S2. Surface temperature and the difference of CO_2 conversion of direct and indirect illumination over Cs-promoted In_2O_3 catalyst

Reaction condition	Surface temperature[a] (°C)	Surface temperature[b] (°C)	Difference of CO_2 conversion Δ(%)
Light	233	230	84.8
Light+250°C	315	311	60.8
Light+300°C	358	353	34.4

[a]: direct illumination; [b]: indirect illumination cover Ti_2O_3

Table S3. Surface temperature of direct and indirect light illumination under different light intensities over Cs-promoted In_2O_3 catalyst.

Light intensity (W·cm⁻	Surface temperature[a] (°C)	Surface temperature[b] (°C)
3.3	315	312
3	307	303
2.52	295	291
2.15	284	280
1.75	275	273
1.37	266	264

[a]: direct illumination; [b]: indirect illumination cover Ti_2O_3

Table S4. Performance comparison of different photocatalysts for CO_2 hydrogenation

Catalyst	$H_2 : CO_2$	Reactor type	Light source	P	T (°C)	CO production (mmol·g⁻¹·h⁻¹)	CO Selectivity	Ref.
Cs/In_2O_3	4 : 1	flow	300W Xe lamp	1 bar	230[a]	**28**	100%	this work
		flow	300W Xe lamp + 250 °C	1 bar	303[a]	**38**	100%	
		flow	300W Xe lamp + 250 °C	10 bar	298[a]	**67**	100%	
		flow	300W Xe lamp + 300 °C	10 bar	345[a]	**74**	100%	
Fe/Al_2O_3	4 : 1	batch	300W Xe lamp	-	310	20	95.96%	1
$2\%Ni\text{-}LaInO_3$	4 : 1	flow	3 W/cm²	-	-	26	100%	2
In_2O_{3-x}	1 : 1	batch	300W Xe lamp	-	340	103.21	100%	3
$Bi_xIn_{2-x}O_3$	1 : 1	batch	300W Xe lamp	30 psi	-	8	-	4
$In_2O_{3-x}(OH)_y/Nb_2O_5$	1 : 1	batch	300W Xe lamp	27 psi	-	1.4	100%	5

In_2O_{3-x}/In_2O_3	1 : 1	batch	300W Xe lamp	30 psi	-	23.88	100%		6
	1 : 1	flow		1 bar	300	0.16 mmol·m^{-2}·h^{-1}	100%		
$In_2O_{3-x}(OH)_y/SiNW$	1 : 1	batch	300W Xe lamp	2 atm	150	0.022	100%		7

[a]Surface temperature

Reference

1. X. Meng, T. Wang, L. Liu, S. Ouyang, P. Li, H. Hu, T. Kako, H. Iwai, A. Tanaka and J. Ye, *Angew. Chem. Int. Ed.*, 2014, **53**, 11478-11482.
2. J. Yu, A. Muhetaer, X. Gao, Z. Zhang, Y. Yang, Q. Li, L. Chen, H. Liu and D. Xu, *Angew. Chem. Int. Ed.*, 2023, e202303135.
3. Y. Qi, L. Song, S. Ouyang, X. Liang, S. Ning, Q. Zhang and J. Ye, *Adv. Mater.*, 2020, **32**, 1903915.
4. T. Yan, N. Li, L. Wang, W. Ran, P. N. Duchesne, L. Wan, N. T. Nguyen, L. Wang, M. Xia and G. A. Ozin, *Nat. Commun.*, 2020, **11**, 6095.
5. H. Wang, J. Jia, L. Wang, K. Butler, R. Song, G. Casillas, L. He, N. P. Kherani, D. D. Perovic and L. Jing, *Advanced Science*, 2019, **6**, 1902170.
6. L. Wang, Y. Dong, T. Yan, Z. Hu, F. M. Ali, D. M. Meira, P. N. Duchesne, J. Y. Y. Loh, C. Qiu and E. E. Storey, *Nat. Commun.*, 2020, **11**, 2432.
7. L. B. Hoch, P. G. O'Brien, F. M. Ali, A. Sandhel, D. D. Perovic, C. A. Mims and G. A. Ozin, *Acs Nano*, 2016, **10**, 9017-9025.